International Journal of Engineering Research & Technology (IJERT)
ISSN: 2278-0181
Vol. 11 Issue 06, June-2022

Modeling a Permanent-Magnet Generator Set under Nonlinear Load

Jose A. Rodriguez
Center for Pulsed Power and Power Electronics,
Texas Tech University
Lubbock, TX

Stephen B. Bayne
Center for Pulsed Power and Power Electronics,
Texas Tech University
Lubbock, TX

***Abstract*— The increasing presence of power electronics in the AC network generates current harmonics that cause adverse effects such as increased power losses and disruption to the control systems of generator sets. This paper proposes a simulation model for a 3-kW diesel-driven permanent magnet generator (PMG) set with MATLAB/Simulink. A testbed was developed to operate the PMG while operating a variable frequency drive (VFD) load while its output voltage, current, and stator temperature were monitored and collected. The configuration of the testbed, method of data collection, and electrical characteristics of the VFD load are presented. The subsystems of the PMG, variable frequency drive load, and a thermal model for the stator windings of the permanent magnet alternator (PMA) were developed. The simulation results are then verified with the empirical data for accuracy. This paper presents a methodology to develop a simulation that can model the behavior of the PMG under nonlinear loads (NLL) and can act as a tool to expand further study into the impact of nonlinear loads on generator sets.**

Keywords*— *Generator set; modeling; power generation; nonlinear loads; current harmonics;

I. INTRODUCTION

It is well understood that current harmonics can cause several issues on AC sources such as generator sets, including increased power losses leading to excessive heating and premature fault trips in control systems [1]. These current harmonics can originate from a power electronic load that typically behave as nonlinear load (NLL). NLLs consist of any loads with nonlinear V-I characteristics and typically have a true power factor below unity due to the presence of reactive power and distortion power generated by the load. Misconceptions about power quality have aided in a rule of thumb where generator sets are typically oversized by establishing their output power capability double the expected power demand of the load [2]. The significant overhead is unavailable in applications where smaller generator sets are desirable, or a size constraint exists, such as establishing a small AC microgrid during an emergency. The issue of power quality is usually addressed by implementing passive or active filtering for improved power quality on the load. There is ongoing research to develop topologies with active filter capabilities to mitigate current harmonics in power electronic systems [3-6]. Still, these measures may not be present in all power electronic systems, especially in older systems. Thus these generator sets are more susceptible to the harmful effects of current harmonics. It is necessary to determine the capabilities of these generator set by investigating their electrical and thermal characteristics.

Previous works have extensively focused on developing a model for just the alternator of a generator set. X. Li et al. have developed a model for a permanent magnet alternator using equations in the stator reference frame [7]. Simulations of three-phase synchronous generators for microgrid applications were demonstrated in [8,9]. Several other works implement high level generator set models that calculate voltage and current averages to simulate controls under microgrid applications [10,11]. The work presented by C. I. Hill et al. is the mode extensive as it includes a set of models for a diesel generator using MATLAB/Simulink [12]. Their research found that their model based on the DQ frame was the best compromise between accuracy and computational cost. The selected generator set unit for this work consist of a diesel engine, alternator and power electronics system, so the proposed simulation work uses a model of the alternator in the stator reference frame and non-switching models for the power electronics to support voltage and current time-varying waveforms. The proposed simulation work includes a model of the NLL that acts as a test load and a source of current harmonics for the generator set unit. As current harmonics can generate excessive power draw, the proposed simulation work also includes a thermal model for the stator windings of the alternator as one indication of its impact to the generator set unit.

This paper focuses on developing a model for a diesel-driven permanent magnet generator (PMG) set to simulate its electrical and thermal characteristics. It presents the testbed where the generator set was operated under an NLL for characterization. The generator set and the NLL are then modeled in MATLAB/Simulink. The proposed simulation is validated experimentally using data from the testbed, which can

Effort sponsored by the U.S. Government under Other Transaction number W15QKN- 09-9-1001/W15QKN-12-9-0001/W15QKN-14-9-1001 between the National Armaments Consortium and the Government. The US Government is authorized to reproduce and distribute reprints for Governmental purposes notwithstanding any copyright notation thereon. The views and conclusions contained herein are those of the authors and should not be interpreted as necessarily representing the official policies or endorsements, either expressed or implied, of the U.S. Government.

International Journal of Engineering Research & Technology (IJERT)
ISSN: 2278-0181
Vol. 11 Issue 06, June-2022

be utilized to investigate the impact of current harmonics, such as the degradation of generator set lifetime.

II. EXPERIMENTAL TESTBED

A testbed was developed to operate the PMG with a variable frequency drive (VFD) load as the NLL. The MEP-831A PMG was selected for this study. The PMG was designed for establishing small AC networks in military applications, but it has been plagued with reliability issues. It uses a 4.4 kW diesel engine to drive a three-phase permanent magnet alternator (PMA) with a power rating of 3.3 kW. The PMA then powers a power electronics converter (PEC) to output a single-phase 120 VAC / 240 VAC at 60 Hz with a power rating of 3 kW [13]. The VFD drives a dynamo to couple power to a three-phase AC network. Fig. 1 shows a block diagram of the testbed for the PMG with the VFD load. A sensor board was developed to measure the output line-neutral voltages, output phase currents of the PMG. For temperature monitoring, the sensor board uses platinum resistance temperature detectors (RTDs) placed around the end-windings of the PMA to measure stator winding temperature. Fig. 2 shows the testbed with the PMG, the operator who monitors the test site, and several NLLs present. These NLLs include a lighting structure using magnetic ballasts, two full-bridge rectifier loads with separate DC loads, and a commercial battery charger, and were implemented as an effort to collect empirical data from the PMG while driving NLLs [14]. The VFD load was selected for this simulation work because it draws the most power from the generator set, can be adjusted to operate in different power levels, and generates the lowest true power factor among the NLLs.

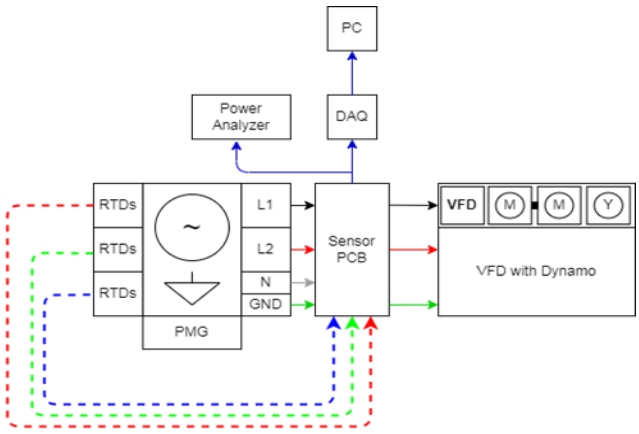

Fig. 1. Block diagram for PMG testbed.

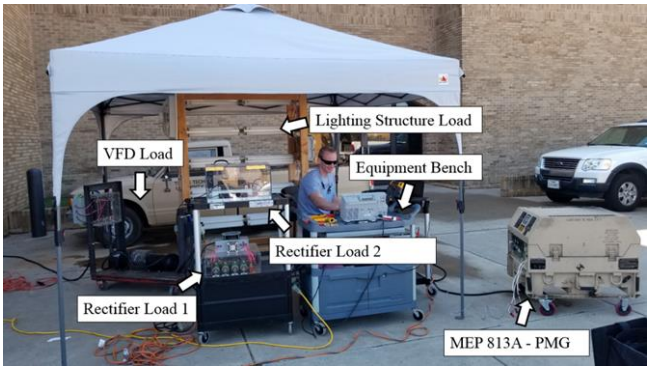

Fig. 2. Image of the PMG testbed.

The VFD load uses an ATV12HU22M2 commercial variable frequency inverter driving a dynamo consisting of two three-phase 3 kW/208 V induction machines to deliver power to an AC network. The power demand of the VFD load can be set with the inverter's frequency. Fig. 3 shows the PMG's output voltage and current with the VFD load, while fig. 4 shows the frequency spectrum of the output current waveform, up to the tenth harmonic. The maximum apparent power draw is 2.6 kVA and the maximum real power draw of the VFD load is 1.48 kW.

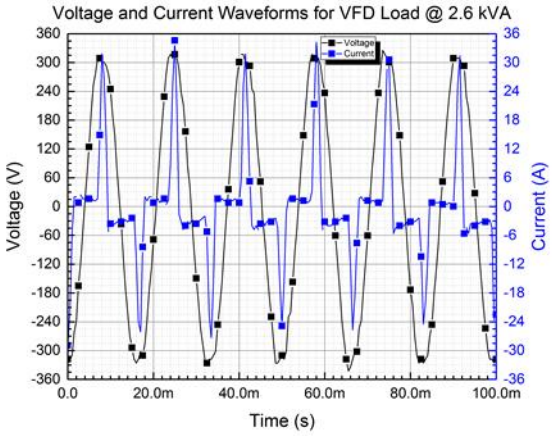

Fig. 3. Voltage and current waveforms with VFD load.

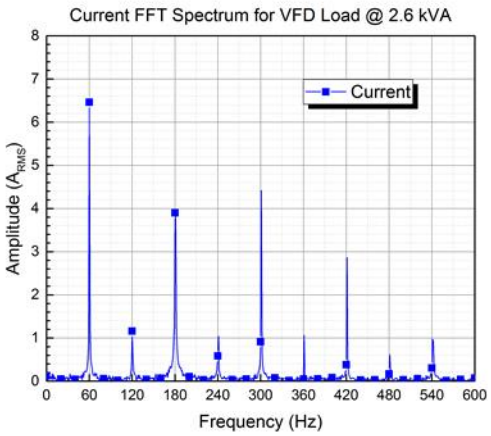

Fig. 4. Spectrum of current waveform with VFD load.

III. SIMULINK MODEL

A PMG and VFD load model was developed in MATLAB/Simulink using a combination of components from the Simscape and specialized power systems library. Figure 5 shows the layout of the Simulink model, with the PMG model consisting of the diesel engine, alternator, and inverter subsystem.

International Journal of Engineering Research & Technology (IJERT)
ISSN: 2278-0181
Vol. 11 Issue 06, June-2022

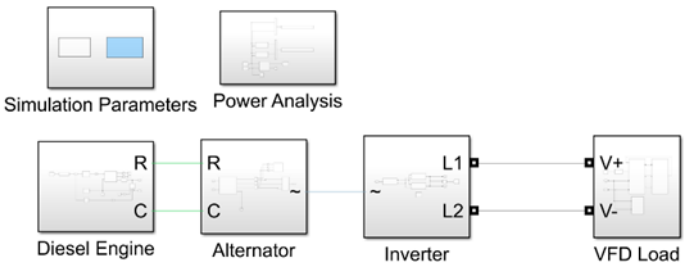

Fig. 5. Simulink model structure.

The 4.9-kW Yanmar L70AE diesel engine from the PMG is modeled using an engine block from the Simscape library. The alternator subsystem uses a permanent magnet synchronous motor (PMSM) block to model the 10-pole three-phase wye configuration PMA with a line-line voltage and power rating of 200 V_{RMS} and 3.3 kW at 376 rad/s [13]. Table 1 shows a compilation of parameters provided from [13] or measured from the PMA.

The PMA was characterized to determine the flux and stator inductance parameters for the PMSM block. A no-load voltage test was performed by removing the PEC and operating the PMG in an open-loop condition, driving the PMA up to 392 rad/s and resulting in an output line-line voltage of 230 V_{RMS}. The linked flux of the PMA is calculated using equation (1):

$$\varphi = \frac{\sqrt{2} * V_{ll,nl}}{\sqrt{3} * P_p * \omega_{m,nl}} \quad (1)$$

The PMSM block requires the self-phase inductance L_s and the mutual inductance M_s. The self-phase inductance was determined by using the equivalent per phase circuit [15] and the resulting equation for L_s is (2):

$$L_s = \frac{((U_{phase} - V_{phase} - R_s * I_{phase})}{2 * \pi * I_{phase} * f_{sync}} \quad (2)$$

The mutual inductance is the difference between the mains inductance and the self-phase inductance [16] and the equation for M_s is (3):

$$M_s = \frac{2 * \mu_0 * M * C_l * t_P * N^2}{\pi^2 * P_p * A_g} - L_s \quad (3)$$

TABLE I. PARAMETERS OF PMA.

Name	Symbol	Unit	Value
Induced voltage	U_{phase}	V	127
Phase voltage	V_{phase}	V	115
Phase current	I_{phase}	A	11.9
Output frequency	f_{sync}	Hz	300
Turns	N	Unitless	15
No-load speed	$\omega_{m,nl}$	rad/s	392
No-load voltage	$V_{ll,nl}$	V	230
Linked Flux	ψ	mWb	96.5
Stator resistance	R_s	mΩ	87.1
Pole pitch	t_P	mm	40.1
Core length	C_l	mm	400
Air gap	A_g	mm	0.254
Pole pair	P_P	Unitless	5
Phases	M	Unitless	3

The temperature of the stator windings is modeled by the PMA thermal model using a lumped parameter thermal model (LPTM). An LPTM can be utilized to perform thermal analysis of the stator assembly [17]. A. Boglietti et al. present several cases where desirable accuracy can be achieved with low order LPTM [18,19]. The LPTM implemented is a third-order RC circuit, where the thermal capacitance corresponds to the stator windings, stator assembly, and rotor mass. The PMA thermal model determines the power dissipation in the windings using a subsystem block that monitors the phase currents of the PMA and calculates the total joule losses. Experimental testing of the PMG without a load shows that the temperature of the windings still increases, due to additional losses on the rotor such as core losses. The second power source is included with a constant power to model this behavior. Table II shows the list of measured dimensions and thermal parameters for calculating the thermal capacitances of the circuit [16],[17]. Equations (4) through (6) calculate the thermal capacitance of the stator windings, stator assembly, and rotor, respectively. Equations (7) through (9) calculate the thermal resistances R2, R3, and R4 of the PMA thermal model. The thermal resistance R1 was tuned to match the steady-state temperature rise on the empirical data. Figure 6 shows the LPTM of the stator windings.

$$C_{th,W} = 0.5 * c_w * P_w * M * S_c * N * L \quad (4)$$

$$C_{th,S} = 0.5 * c_s * P_s * \pi * L * ({r_{stator}}^2 - {r_{gap}}^2) \quad (5)$$

$$C_{th,R} = 0.5 * c_r * P_r * \pi * L * ({r_{rotor}}^2 - {r_{shaft}}^2) \quad (6)$$

$$R_2 = \frac{1}{\pi * h_c * L * r_{rotor}} \quad (7)$$

$$R_3 = \frac{1}{h_{gap} * \pi * {r_{gap}}^2} + \frac{1}{\pi * L * (0.5 * r_{gap} * h_{teeth} + k_i * 4 * M * N)} \quad (8)$$

$$R_4 = \frac{1}{\pi * h_{shaft} * L * r_{shaft}} \quad (9)$$

TABLE II. THERMAL PARAMETERS OF LPTM.

Name	Symbol	Unit	Value
Winding specific heat	C_w	J/(Kg*K)	385
Stator specific heat	C_s	J/(Kg*K)	500
Rotor specific heat	C_r	J/(Kg*K)	370
Winding Density	P_w	Kg/m^3	8.94*10^3
Stator Density	P_s	Kg/m^3	7.87*10^3
Rotor Density	P_r	Kg/m^3	8.40*10^3
Length of PMA	L	mm	102
Cross-area of wire	S_c	mm^2	3.08

International Journal of Engineering Research & Technology (IJERT)
ISSN: 2278-0181
Vol. 11 Issue 06, June-2022

Radius of shaft	r_{shaft}	mm	12.7
Radius of rotor	r_{rotor}	mm	63.5
Inner radius of stator	r_{gap}	mm	63.8
Outer radius of stator	r_{stator}	mm	88.9
Thermal conductance of winding insulation	k_i	W/(K*m)	0.2
Heat flow coefficient, stator to yoke	h_c	W/(K*m^2)	350
Heat flow coefficient, shaft to rotor	h_{shaft}	W/(K*m^2)	430
Heat flow coefficient, air gap	h_{gap}	W/(K*m^2)	10.5
Heat flow coefficient, stator teeth	h_{teeth}	W/(K*m^2)	80

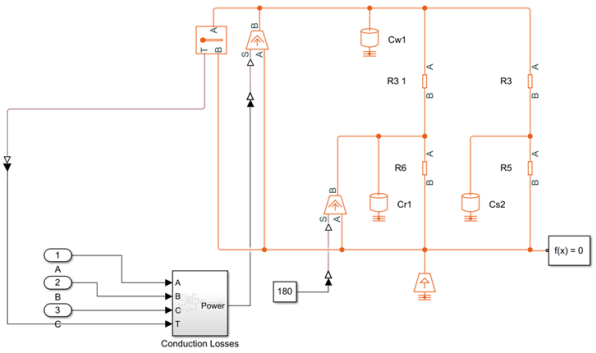

Fig. 6. Third-order LPTM for stator winding.

Fig. 7 shows the half-bridge inverter subsystem, while fig. 8 shows the overall inverter subsystem. The inverter subsystem uses three-phase rectifiers to rectify the PMA's phase voltage and an interface block to transition the model from Simscape components to specialized power systems components for the half-bridge inverters. A controller subsystem measures the bus voltage, filter inductor current, and output voltage of the half bridges for voltage regulation. The half-bridge inverters use non-switching half-bridge modules to improve computational cost. An LCLC filter is implemented which is found on the PEC. The inductors L1 and L2 have a value of 145 µH and 60 µH, respectively, and capacitor C11 and C12 have the same value of 40 µF.

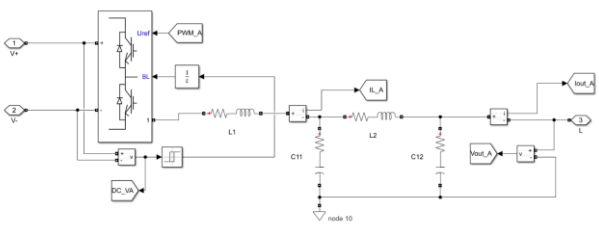

Fig. 7. Half-bridge inverter subsystem structure.

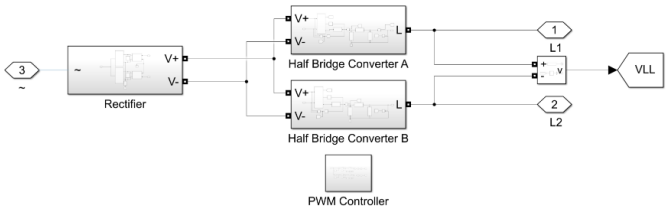

Fig. 8. Inverter subsystem structure.

Figure 9 shows the layout of the VFD load subsystem. A subsystem for the VFD load was also developed using specialized power system components. The VFD load subsystem implements a single-phase rectifier to power a three-phase inverter. The three-phase inverter uses an average non-switching model block with space vector modulation. The inverter then drives a dynamo consisting of two induction machines, feeding power into a three-phase source that acts like the AC network load. Figure 10 shows the layout of the dynamo. The parameters of the induction machines were extracted from their datasheets. An inner feedback loop is implemented to regulate the rotor speed of the inductive motor to a reference point controlled by an outer feedback loop to obtain the desired apparent power draw. It was observed that the apparent power draw of the VFD load peaks after ramping up and gradually decreases before reaching a final steady-state value. The feedback loop models this behavior by initially setting the desired reference point 40 % above the desired steady state value. The final steady-state apparent power draw is adjusted by tuning the three-phase inverter frequency.

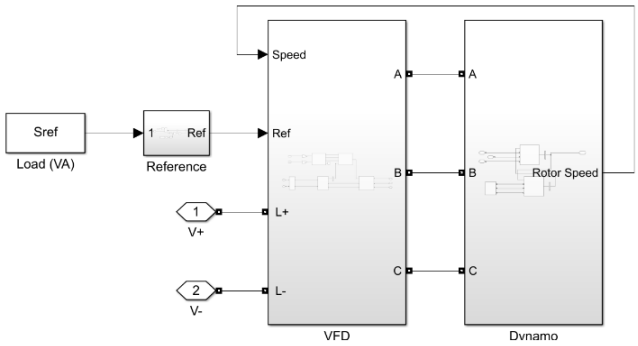

Fig. 9. VFD load subsystem structure.

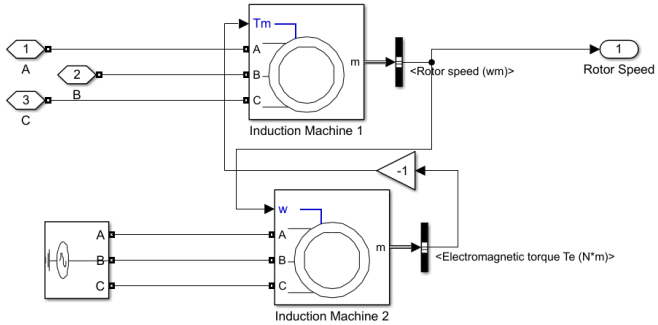

Fig. 10. VFD dynamo subsystem structure.

IV. DISCUSSION

The results from the simulation were compared with the collected empirical data. The empirical data was collected during a four hour test interval. Figure 11 compares the measured apparent power from the empirical data with the

International Journal of Engineering Research & Technology (IJERT)
ISSN: 2278-0181
Vol. 11 Issue 06, June-2022

apparent power of the simulation. The average apparent power of the empirical data at the end of the testing interval is 2.16 kVA, while for the simulation, it is just slightly above 2.17 kVA. Figure 12 compares the temperature rise from the empirical data and the simulation data. A steady-state temperature value of 50.5 ˚C was measured from the empirical data, while the simulation achieved a temperature rise of 51.2 ˚C.

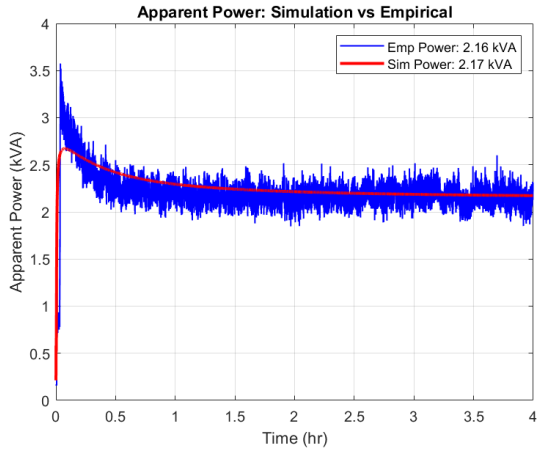

Fig. 11. Comparison of apparent power over time.

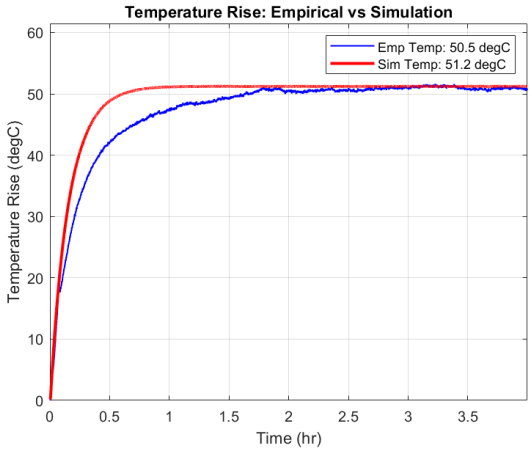

Fig. 12. Comparison of temperature rise over time.

Figure 13 shows the output current frequency spectrum of the empirical data, while figure 14 shows the output current frequency spectrum of the simulation data. For both figures, the frequency spectrum was calculated using data with equivalent of 100 cycles. The THD of the empirical data is 1.24, whereas the simulation data has a THD of 1.39. The resulting distortion power factor for the empirical and simulation data is 0.62 and 0.58, and with the displacement power factor of 0.98 and 1.0 for the empirical and simulation data, the true power factor is 0.61 and 0.58, respectively. Along with odd and even harmonics, there are also subharmonics present in figure 13 that may result from fluctuations of the rotor speed feedback loop on the VFD load, causing additional distortions in the current waveform.

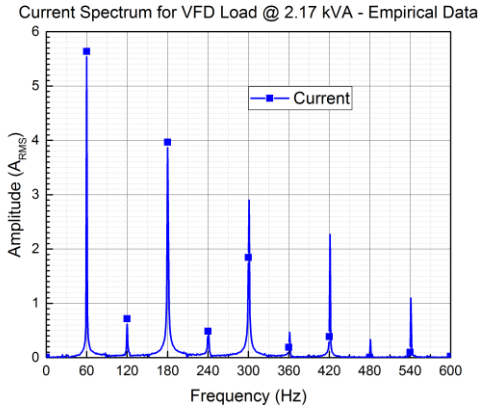

Fig. 13. Spectrum of current waveform from empirical data.

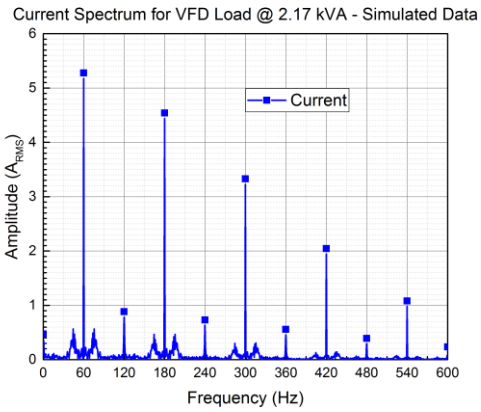

Fig. 14. Spectrum of current waveform from simulation result.

The presence of the current harmonics increases the apparent power demand of the NLL, subjecting the PMA and the PEC to increased current circulation. Although the input capacitors from the PEC acts as a buffer for the current harmonics generated by the NLL, the increased current draw due to current harmonics from the NLL also increases the current draw and power dissipation in the PMA. The expected lifetime of the PMG can be estimated by considering the continuous operating temperature of its stator windings [20]. The thermal model was implemented into the PMG model to simulate the operating temperatures of the winding while considering its load. Figure 15 compares the temperature rise in the simulation with the VFD load and a resistive load with the equivalent real power draw of the VFD load. The presence of current harmonics causes a temperature increase of 7.8 degrees in the PMA.

International Journal of Engineering Research & Technology (IJERT)
ISSN: 2278-0181
Vol. 11 Issue 06, June-2022

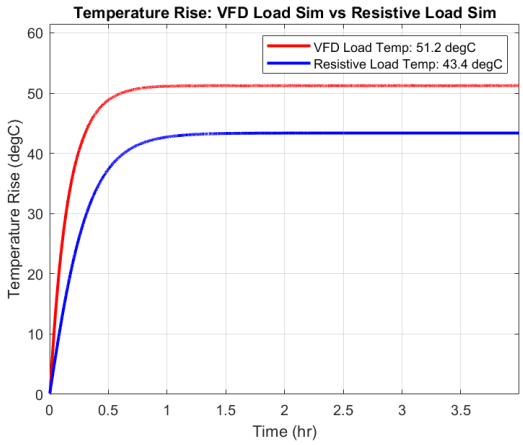

Fig. 15. Comparison of temperature rise over time.

V. CONCLUSION

This paper presented the development of a simulation model for a generator set as a tool to study the effects of current harmonics. For characterization, a testbed was developed to operate a generator set under a non-linear load. An electrical model of the generator set and its non-linear load from the testbed were developed. The model includes major subsystems to allow probing of each stage. Several model instances can run in parallel with different NLLs in Simulink. A thermal model of the stator windings was included to show the temperature rise of the windings during operation. The temperature rise can be used to determine the degradation in the generator's lifetime set for a given NLL. The proposed simulation model can be utilized for power quality analysis for any load type, and the procedure presented can be implemented in any generator set. The simulation work can be further expanded by testing the PMG with different NLLs and incorporating them into the simulation to model the PMG driving an AC network of expected loads.

REFERENCES

[1] C. Thomas H. Ortmeyer, K. R. Chakravarthi and A. A. Mahmoud. THE EFFECTS OF POWER SYSTEM HARMONICS ON POWER SYSTEM EQUIPMENT AND LOADS. IEEE Transactions on Power Apparatus and Systems Vol. PAS-104, No. 9, 1985.

[2] S. Basak, A. K. Mondal and C. Chakraborty. Performance and Analysis of a New Brushless Synchronous Generator for DC Microgrid Application. IEEE Transactions on Industry Applications vol. 56, no. 3, pp. 3137-3148, May-June 2020, doi: 10.1109/TIA.2020.2974444.

[3] W.-T. Kao, J.-C. Hwang, and J.-E. Liu. Development of Three-Phase Permanent-Magnet Synchronous Motor Drive with Strategy to Suppress Harmonic Current. Energies, vol. 14, no. 6, p. 1583, Mar. 2021.

[4] K. -W. Wang, K. Zhang, C. -P. Tung and H. S. -H. Chung. Active Bridge Rectifier With DM EMI Reduction Based on Linear Reverse Operation of MOSFETs. IEEE Transactions on Power Electronics vol. 36, no. 3, pp. 2971-2982, March 2021, doi: 10.1109/TPEL.2020.3013629.

[5] Z. Miao, H. Tong, X. Jin, W. Yao, Z. Lu and Z. Ma. DQ-Frame Zero-Crossing Effect Modeling and Current Distortion Compensation Method for Vienna Rectifier. IEEE Transactions on Power Electronics vol. 35, no. 7, pp. 7612-7623, July 2020, doi: 10.1109/TPEL.2019.2957540.

[6] I. Bouloumpasis, P. Vovos, K. Georgakas, and N. Vovos. Current Harmonics Compensation in Microgrids Exploiting the Power Electronics Interfaces of Renewable Energy Sources. Energies, vol. 8, no. 4, pp. 2295–2311, Mar. 2015.

[7] H. Hoevenaars, M. McGraw and J. Alexander. Rightsizing Generators Through Harmonic Mitigation Realizes Energy, Emissions, and Infrastructure Reductions. IEEE Transactions on Industry Applications vol. 53, no. 1, pp. 675-683, Jan.-Feb. 2017, doi: 10.1109/TIA.2016.2603143.

[8] Li, X.; Chau, K.T.; Wang, Y. Modeling of a Field-Modulated Permanent-Magnet Machine. Energies 2016, 9, 1078. https://doi.org/10.3390/en9121078

[9] L. G. Weber, A. Nasiri and H. Akbari. Dynamic Modeling and Control of a Synchronous Generator in an AC Microgrid Environment. IEEE Transactions on Industry Applications vol. 54, no. 5, pp. 4833-4841, Sept.-Oct. 2018, doi: 10.1109/TIA.2018.2845392.

[10] Corsini, A.; Cedola, L.; Lucchetta, F.; Tortora, E. Gen-Set Control in Stand-Alone/RES Integrated Power Systems. Energies 2019, 12, 3353. https://doi.org/10.3390/en12173353

[11] B. Singh, G. Pathak and B. K. Panigrahi. Seamless Transfer of Renewable-Based Microgrid Between Utility Grid and Diesel Generator. IEEE Transactions on Power Electronics vol. 33, no. 10, pp. 8427-8437, Oct. 2018, doi: 10.1109/TPEL.2017.2778104.

[12] C. I. Hill, P. Zanchetta, and S. V. Bozhko. Accelerated Electromechanical Modeling of a Distributed Internal Combustion Engine Generator Unit. Energies, vol. 5, no. 7, pp. 2232–2247, Jul. 2012.

[13] Operator, Unit, and Direct Support Maintenace Manual 3kW Tactical Quiet Generator Set MEP-831A (60 Hz),Departments of the Army and the Air Force And Headquarters, Marine Corps, 2005.

[14] J. Rodriguez, S. Fernando, S. Bayne. "Investigating the Effects of Non-Linear Loads on Generator Sets" 2021 IEEE Pulsed Power and Plasma Science Conference.

[15] S. Chapman, Electric Machinery Fundamentals, McGraw Hill, 2012.

[16] J. Pyrhonen, T. Jokinen, V. Hrabovcova, Design of Rotating Electrical Machines, John Wiley & Sons, 2008.

[17] P. Mellor, D. Roberts, D. Turner. Lumped parameter thermal model for electrical machines of TEFC design. IEE Proceedings B (Electric Power Applications) vol. 138, no. 5, September 1991. DOI: 10.1049/ip-b.1991.0025

[18] A. Boglietti, E. Carpaneto, M. Cossale and S. Vaschetto. Stator-Winding Thermal Models for Short-Time Thermal Transients: Definition and Validation. IEEE Transactions on Industrial Electronics vol. 63, no. 5, pp. 2713-2721, May 2016, doi: 10.1109/TIE.2015.2511170.

[19] A. Boglietti, M. Cossale, S. Vaschetto and T. Dutra. Winding Thermal Model for Short-Time Transient: Experimental Validation in Operative Conditions. IEEE Transactions on Industry Applications vol. 54, no. 2, pp. 1312-1319, March-April 2018, doi: 10.1109/TIA.2017.2777920.

[20] A. Elsebaay, M. A. A. Adma and M. Ramadan, "Analyzing the Effect of Ambient Temperature and Loads Power Factor on Electric Generator Power Rating," International Journal of Energy and Power Engineering, 2017.